An Ultrasonic Mode Conversion Technique for Characterizing Prism-Shaped Material Samples – Experimental and Numerical Results

Abdelmalek BOUHADJERA, NDT Lab, Jijel University, Algeria
Frank SCHUBERT, Fraunhofer-IZFP, Dresden Branch, Germany

Abstract. An ultrasonic apparatus based on a mode conversion technique is described. It involves the measurement of the velocity of both compressional and shear waves in prism shaped specimens with only one transducer. The shear waves are generated through mode conversion at the interface between water and the specimen under test. The optimum coupling of the transducer and the special arrangement of the specimen enable the evaluation of not only second order elastic constants, but third order elastic constants as well, since the specimen can be easily subjected to both compressive and hydrostatic pressure. Preliminary experimental results obtained using different isotropic materials and numerical simulations of wave propagation based on the elastodynamic finite integration technique (EFIT) are presented. The results reveal that the prism technique is a significant improvement compared to traditional goniometer and rotating plate techniques.

Introduction

Measurements of sound velocities have great practical importance since they lead to the determination of elastic material constants from well-known formulae. There are various methods based on through-transmission and pulse-echo techniques [1, 2].

Provided that compressional waves (P waves) can be set up within a liquid medium, both compressional and shear waves (S waves) can be generated in a solid specimen by a mode conversion process that takes place upon refraction at a boundary, where an acoustic impedance discontinuity exists. Bar [3] for example, used this principle to measure both P and S wave velocities in solids. Later Schneider and Burton [4] made measurements with the rotating plate technique in which the sample is in the form of a rectangular block, and mounted on a turntable that can be rotated in steps of 0.1 degrees and located between a pair of compression wave probes, one transmitting and the other receiving. The complete arrangement is immersed in a water tank.

Reynolds [5] in his technique used a cylindrical rod. Optical methods of detection are applied with accuracy, being principally limited by the precision with which the angles of the various sound beams in the immersion liquid can be measured. Rao [6] chose conditions such that the angle for incident waves was greater than the critical angle for P waves within the plate. Hence, only S waves were present in the solid. Again, the angle of incidence must be accurately known in order to determine the S wave velocity. This velocity can also be determined by directly observing the diffraction pattern produced by

shear waves within a transparent solid, as reported by Breezeale and Hiedemann [7]. Mayer [8] used the critical-angle method by a goniometer arrangement for determining the velocity of sound in a flat smooth sample. The pronounced amplitude changes at the critical angles permit the reading of angles within 0.1 degrees.

Most old and recent research in this field is based more or less on the same basic principles of the methods mentioned above [9-20]. The drawback with these methods is the angle of rotation, which has to be determined with high accuracy, thus increasing the complexity of the measuring system. The new method described here is an improvement to an immersion technique designed by the main author [21, 22]. Both P and S waves are generated by mode conversion in a prism-shaped specimen. The angle arrangement allows for just one variable to be left in the equation that enables the computation of the velocity of ultrasonic waves [23, 24].

1. Reflection and transmission at a liquid-solid boundary

If a plane sound wave in a liquid strikes a plane interface of a solid obliquely (figure 1), a reflected P wave in the liquid, a refracted P and a mode converted S wave in the solid are generated (see e.g. [1] or [25]).

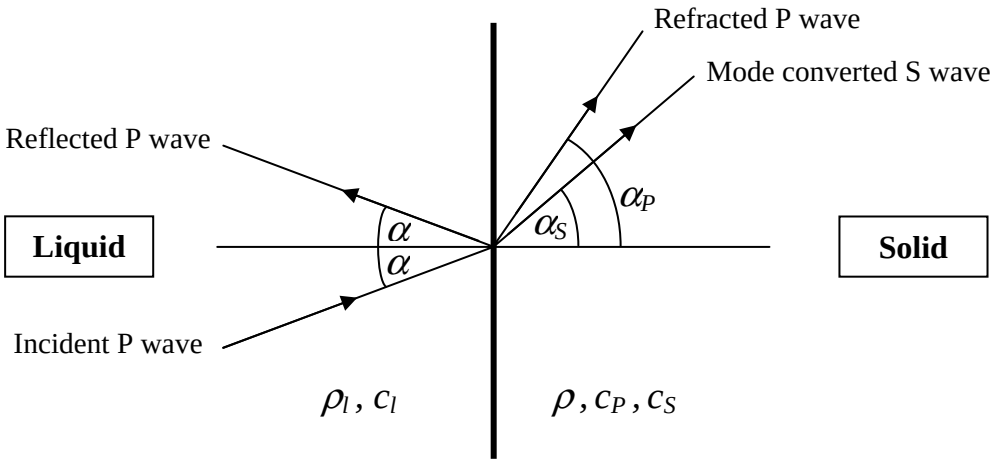

Figure 1: Reflection, refraction, and mode conversion of an obliquely incident P wave at a liquid-solid interface.

The directions of the reflected and transmitted waves are determined by Snell's law,

$$\frac{\sin\alpha}{c_l} = \frac{\sin\alpha_{P,S}}{c_{P,S}} \quad , \tag{1}$$

whereas α is the angle of incidence and simultaneously the angle of the reflected P wave in the liquid, α_P and α_S are the angles of refracted P and S wave in the solid, respectively, and c_l, c_P and c_S are the wave speeds of the P wave in the liquid and of the P and S wave in the solid, respectively. The wave reflection and transmission coefficients with regard to intensity, R, T_P, and T_S, are given by the following equations (e.g. [25]):

$$R(\alpha) = \left(\frac{K - 2Z_l^n}{K} \right)^2 \quad , \tag{2}$$

$$T_P(\alpha) = \frac{4 Z_l^n Z_P^n}{K^2} \cos^2 2\alpha_S \quad , \tag{3}$$

$$T_S(\alpha) = \frac{4 Z_l^n Z_S^n}{K^2} \sin^2 2\alpha_S \quad , \tag{4}$$

with

$$K = Z_P^n \cos^2 2\alpha_S + Z_S^n \sin^2 2\alpha_S + Z_l^n$$

and

$$Z_l^n = \frac{\rho_l \, c_l}{\cos\alpha} \quad , \quad Z_P^n = \frac{\rho \, c_P}{\cos\alpha_P} \quad , \quad Z_S^n = \frac{\rho \, c_S}{\cos\alpha_S} \quad .$$

In these equations, the angles α, α_P, and α_S are linked via equation (1) and conservation of energy requires $R + T_P + T_S = 1$.

In order to discuss the formulae, we choose an elastic half space with ρ = 2133 kg/m³, c_P = 3950 m/s, c_S = 2355 m/s, according to a typical mortar specimen, and use ρ_l = 1000 kg/m³ and c_l = 1470 m/s as material parameters for (distilled) water. Figure 2 shows the different curves calculated by equations (2)-(4).

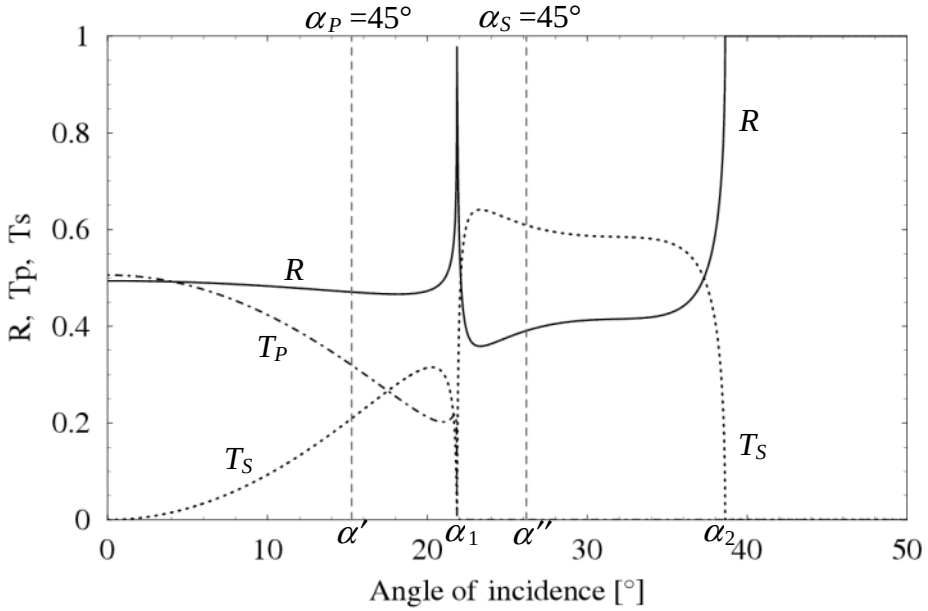

Figure 2: Intensity reflection coefficient, R, transmission coefficient for the refracted P wave, T_P, and transmission coefficient for the mode converted S wave, T_S, as a function of the angle of incidence α for a water/mortar combination (ρ_l = 1000 kg/m³, c_l = 1470 m/s, ρ = 2133 kg/m³, c_P = 3950 m/s, c_S = 2355 m/s).

At an angle of incidence α = 0° only a reflected P wave in the liquid and a transmitted P wave in the solid (with α_P = 0°) exist. In this case, reflection and transmission coefficient with regard to intensity amount to

$$R(0°) = \left(\frac{Z_P - Z_l}{Z_P + Z_l} \right)^2 \tag{5}$$

and

$$T_P(0°) = 1 - R(0°) = \frac{4Z_l Z_P}{(Z_P + Z_l)^2} \quad , \tag{6}$$

in which $Z_l = \rho_l \cdot c_l$ and $Z_P = \rho \cdot c_P$ represent the acoustic impedances of the liquid and the solid medium, respectively. For our water/mortar example we obtain $R\,(0°) = 0.494$ and $T_P(0°) = 0.506$ (compare figure 2).

At increasing angle of incidence, $\alpha > 0$, an additional shear wave with increasing intensity is generated in the solid by mode conversion of the incident P wave. Simultaneously the transmission coefficient of the refracted P wave decreases.

Since in most practical cases the wave speed of the liquid, c_l , is smaller than the wave speeds in the solid, c_P and c_S , the angles of refraction, α_P, α_S, are larger than the angle of incidence, α. Therefore, at a first critical angle of incidence, α_1, the angle of refraction of the P wave in the solid reaches 90° and thus, at this point the P wave disappears from the solid. This first critical angle is given by

$$\alpha_1 = \arcsin\left(\frac{c_l}{c_P}\right) \quad . \tag{7}$$

In our present example this happens at $\alpha_1 = 21.85°$ (see figure 2). At this critical angle of incidence the reflected P wave in the liquid increases significantly with a reflection coefficient close (but not identical) to one.

In the solid for $\alpha > \alpha_1$ the incident P wave is completely transformed into the mode converted S wave. The intensity of the latter rapidly increases at the expense of the reflected P wave. If we further increase the angle of incidence, the angle of refraction of the S wave also reaches 90° and at this point the S wave disappears, too. This second critical angle of incidence, α_2, is given by

$$\alpha_2 = \arcsin\left(\frac{c_l}{c_S}\right) \quad . \tag{8}$$

In our water/mortar example this happens at $\alpha_2 = 38.62°$ (see Fig. 2). For $\alpha > \alpha_2$ the reflection coefficient for the incident P wave in the liquid is equal to one since all other wave modes are no longer present.

2. Basic principles of the prism technique

The main piece of the apparatus is the transducer cell shown in figure 3. It consists of a water tank in which the specimen under test (SUT) is fixed. The single transducer that acts as both transmitter and receiver is put on a circle that turns around SUT with a radius R (about 4 cm). The ultrasonic beam makes an angle α that varies in a continuous manner from 0° to 90°. The main face of SUT is put against the diameter line XX' and has to be placed in such a way that its center coincides with the center of the transducer circle (point O in figure 3). This is done by moving SUT parallel to XX' following the arrows and pointing the right angle of the prism in the direction of the positioning line. The latter is perpendicular to the main prism surface.

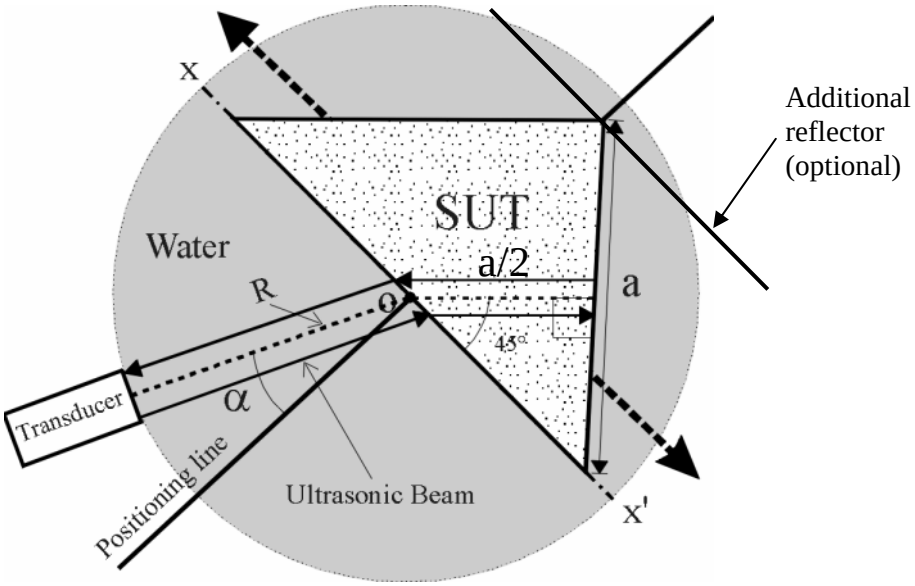

Figure 3: Transducer cell configuration as used for the prism technique.

They key idea of the prism technique is that only waves inside the prism with a refraction angle of 45° significantly contribute to the sensor signal. These refracted waves impinge normally on one of the side faces of the prism with length *a*, are reflected at the prism/water interface, and propagate back to the receiver using exactly the same travel path as before (reciprocity principle). From equation (1) we see that this happens if the angle of incidence is

$$\alpha' = \arcsin\left(\frac{1}{\sqrt{2}}\frac{c_l}{c_P}\right) \tag{9}$$

for the refracted P wave, and

$$\alpha'' = \arcsin\left(\frac{1}{\sqrt{2}}\frac{c_l}{c_S}\right) \tag{10}$$

for the mode converted S wave. For our water/mortar example we obtain α' = 15.26° and α'' = 26.19° (see dashed vertical lines in figure 2). The determination of the elastic constants of the prism material is then based on the following three steps.

2.1 First step: Transit time of reflected P wave

P wave reflection with α_P = 0° from the main face of SUT occurs when the angle of incidence α is equal to zero (normal incidence along the positioning line). This enables the evaluation of time-of-flight $t_P = 2R / c_l$. A numerical simulation of this situation using the elastodynamic finite integration technique (EFIT [26]) is shown in figure 4. According to equation (5) approximately 49% of acoustic energy is reflected back to the transducer. The remaining portion is transferred to the P wave in the prism. In this initial step the transmitted wave in the prism is not needed for evaluation.

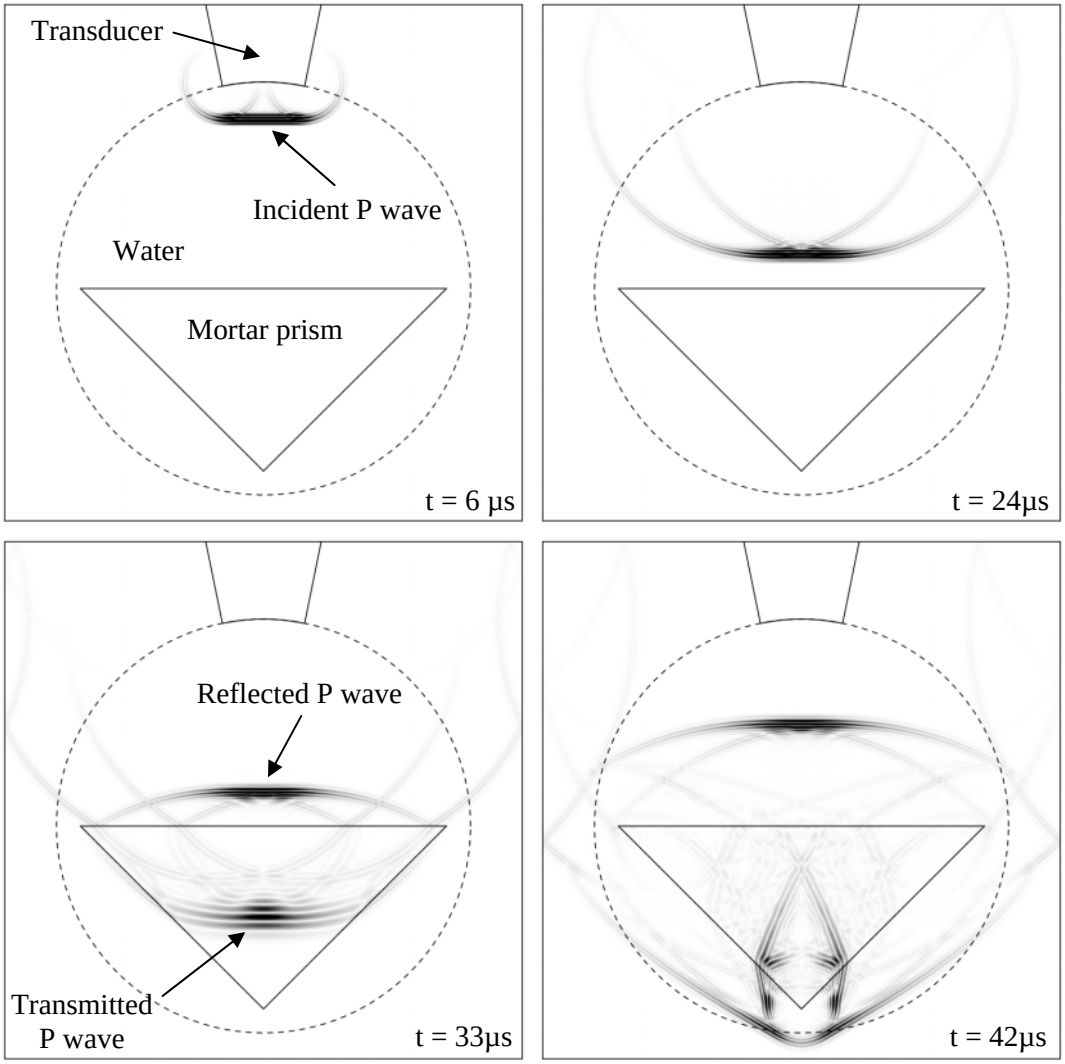

Figure 4: 2-D EFIT simulation of normal incidence case for the water/mortar example (size of the model = 10 × 10 cm, side length of the prism = 5 cm, center frequency of the input pulse = 1 MHz). The wave front snapshots represent the absolute value of particle velocity using a linear grey scale. They were taken at $t \approx 6$, 24, 33, and 42 µs after start of excitation.

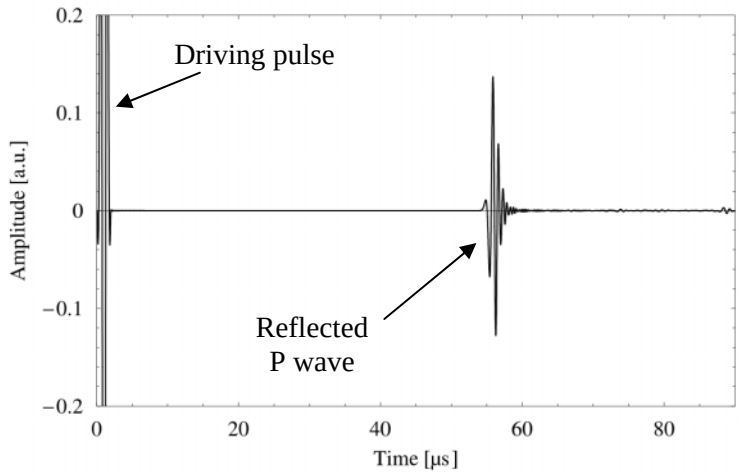

Figure 5: Time-domain signal of normal particle velocity according to figure 4, calculated by integrating over the transducer aperture. From the sensor signal the time-of-flight of reflected P wave, t_P, can be determined (step 1 of the prism technique).

2.2 Second step: Transit time of refracted P wave

By increasing the angle of incidence, the reflected P wave echo disappears, and a second echo appears, which is related to refracted P wave within SUT (due to the finite transducer aperture the ultrasonic beam carries some divergent portions so that refraction angles of 45° always appear even when the main beam is not refracted in the 45° direction). In this region the measured time-of-flight of the refracted P wave echo is independent (!) on the angle of incidence, α, but certainly its amplitude varies with varying α. The maximum echo is obtained if the angle of refraction is 45°, i.e. $\alpha = \alpha'$ according to equation (9). In our water/mortar example this happens at $\alpha' = 15.26°$.

It is worth mentioning once again, that for measurement of the echo transit time it is *not* necessary to exactly adjust α to α'. It is sufficient to manually tune the echo amplitude to obtain a good signal-to-noise ratio. This fact represents a significant improvement over goniometer arrangements where the angle of incidence has to be measured exactly.

A numerical EFIT simulation using an incidence angle of $\alpha = \alpha'$ is shown in the following figure 6.

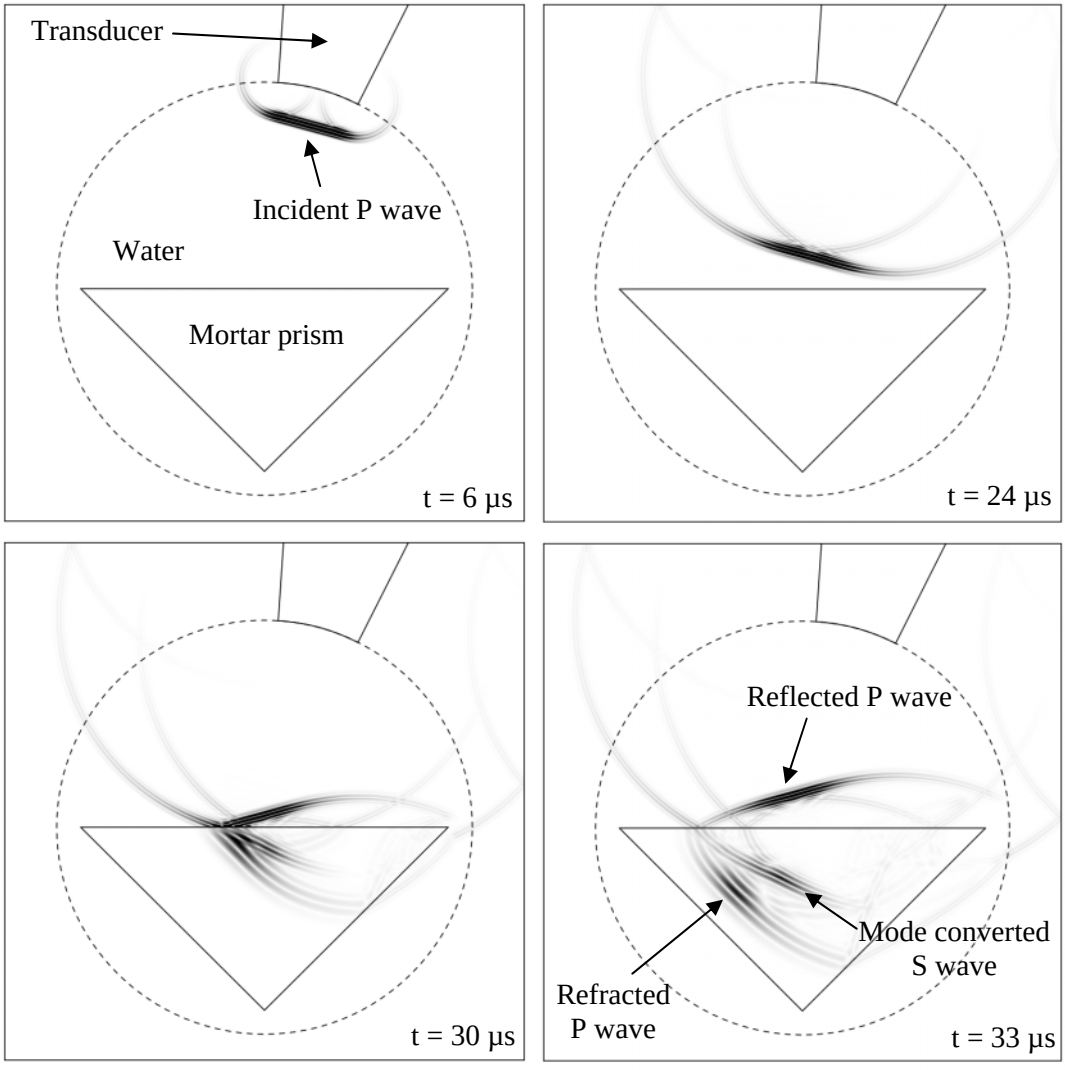

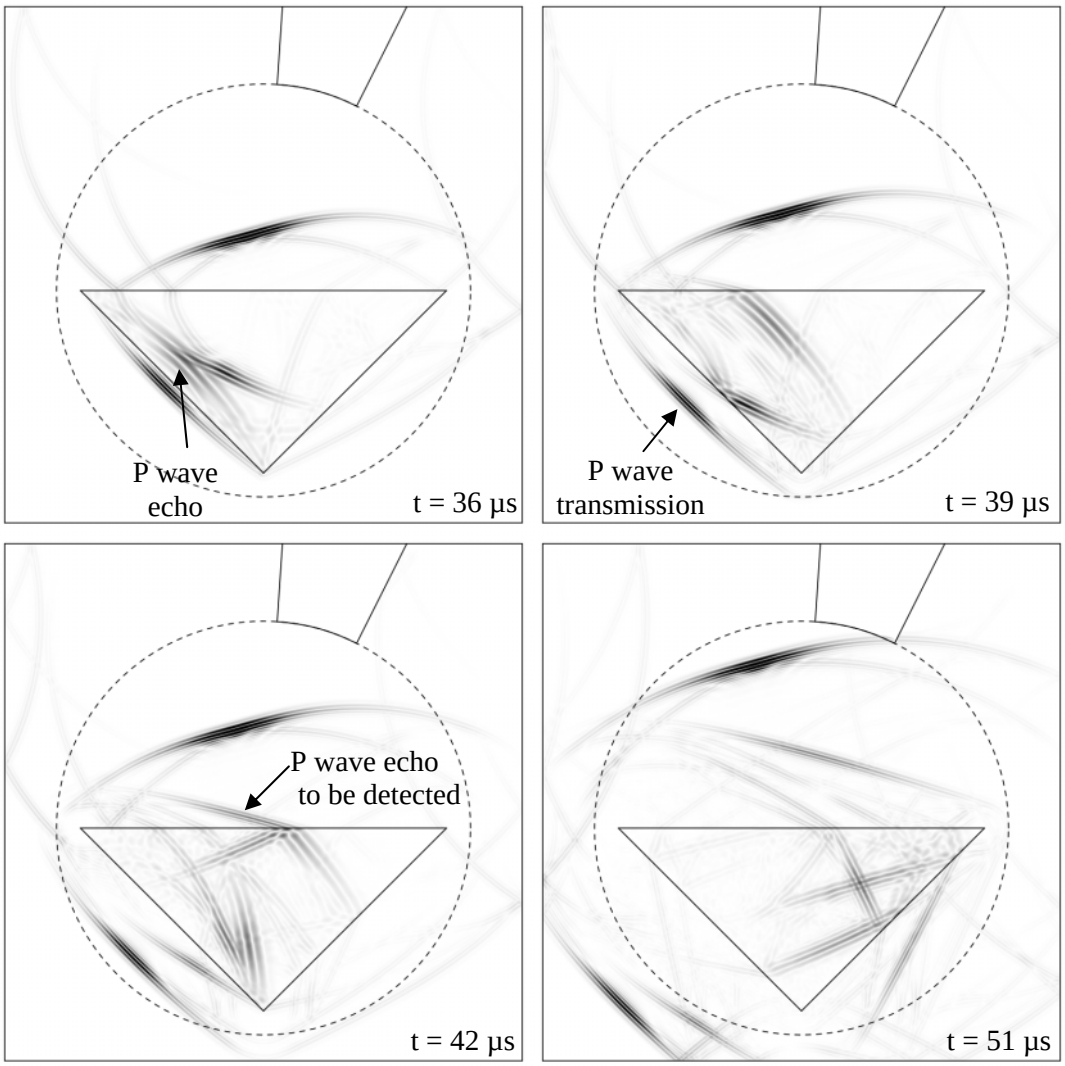

Figure 6: 2-D EFIT simulation for a P wave refraction angle of 45° for the water/mortar example (size of the model = 10 × 10 cm, side length of the prism = 5 cm, center frequency of the input pulse = 1 MHz). The wave front snapshots represent the absolute value of particle velocity using a linear grey scale. They were taken at $t \approx 6$, 24, 30, 33, 36, 39, 42, and 51 µs after start of excitation.

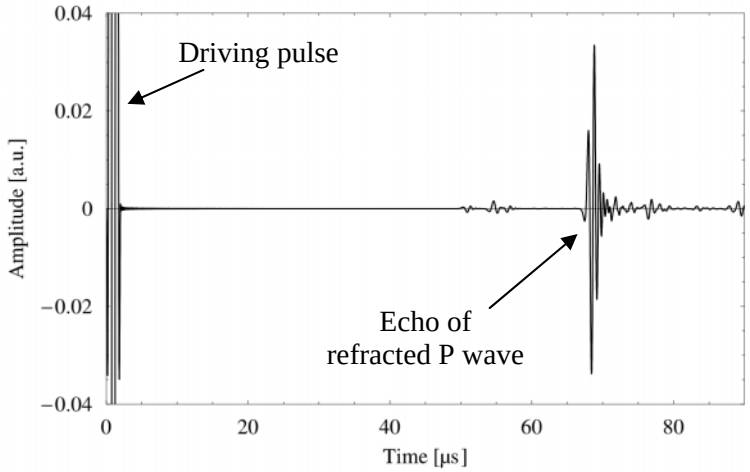

Figure 7: Time-domain signal of normal particle velocity according to figure 6, calculated by integrating over the transducer aperture. From the sensor signal the time-of-flight of the refracted P wave, T_P, can be determined (step 2 of the prism technique).

From the wave front snapshots in figure 6 it can be seen that not only a refracted P wave but also a mode converted shear wave is generated in the prism. However, since the refraction angle of this S wave is significantly smaller than 45° no significant contribution appears in the calculated time-domain signal of particle velocity as shown in figure. 7. The refracted P wave however is partly reflected by the left side face of the prism (normal incidence!), runs back to the main face where it is once again reflected, mode converted, and refracted. Only the refracted part (refraction angle = original incidence angle α!) in the liquid propagates back to the transducer where it produces a well-defined echo signal (see figure 7). From this sensor signal the time-of-flight of the refracted P wave, T_P, can be easily determined.

2.3 Third step: Transit time of mode converted S wave

A further increase of the angle of incidence α makes the P wave echo disappear, and after that a new echo will appear, which is related to the mode converted shear wave in the prism. The maximum echo is obtained if the angle of refraction is 45°, i.e. $\alpha = \alpha''$ according to equation (9). In our water/mortar example this happens at $\alpha'' = 26.19°$. An EFIT simulation of this case is shown in the following figure 8.

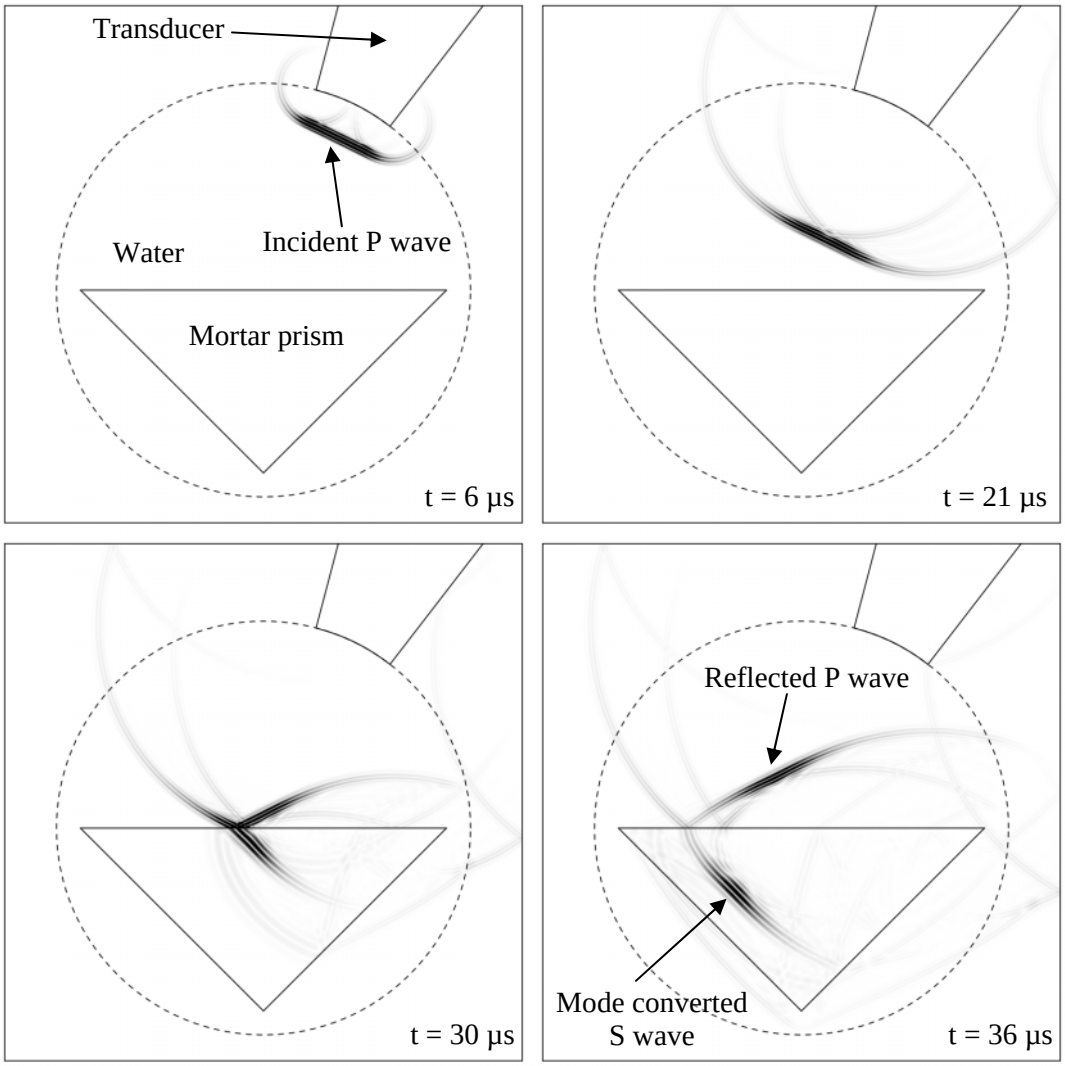

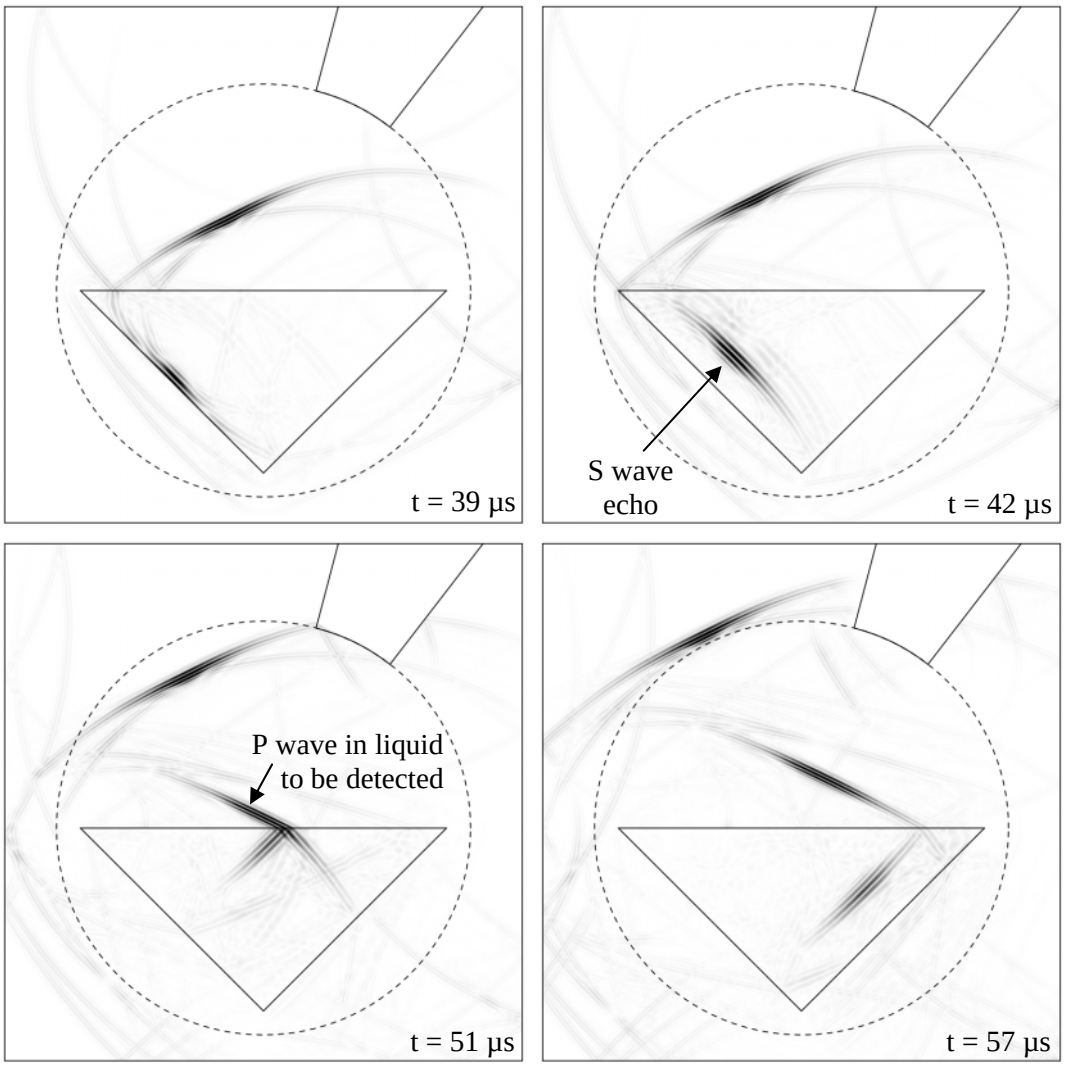

Figure 8: 2-D EFIT simulation for S wave refraction angle of 45° for the water/mortar example (size of the model = 10 × 10 cm, side length of the prism = 5 cm, center frequency of the input pulse = 1 MHz). The wave front snapshots represent the absolute value of particle velocity using a linear grey scale. They were taken at $t \approx 6$, 21, 30, 36, 39, 42, 51, and 57 µs after start of excitation.

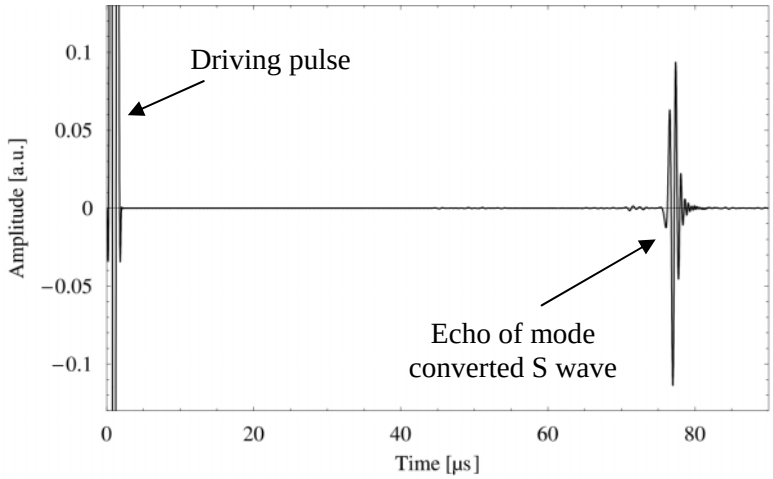

Figure 9: Time-domain signal of normal particle velocity according to figure 8, calculated by integrating over the transducer aperture. From the sensor signal the time-of-flight of the mode converted S wave, T_S, can be determined (step 3 of the prism technique).

The wave front snapshots in figure 8 reveal that inside the prism the incident P wave is nearly completely transformed to the mode converted S wave since in this case the incidence angle α'' is greater than the first critical angle of the P wave, α_1 (compare figure 2). Thus, at least for idealized plane waves no P wave in the prism should exist. Nevertheless, in the third snapshot of figure 8, a weak refracted P wave in the prism can still be observed. This wave is caused by the divergent parts of the incident beam yielding to slightly differing incidence and refraction angles.

A comparison between the signals in figures 7 and 9 shows that the amplitude of the detected S wave echo is significantly larger than that of the P wave echo. Two main facts seem to be responsible for that. First of all, according to figure 2 at $\alpha = \alpha''$ more than 60% of incident acoustic energy is transferred to the refracted S wave. In contrast to that at $\alpha = \alpha'$ only about 32% is transferred to the refracted P wave. Secondly, the reflection of both waves at the side face of the prism (i.e. the mortar/water interface) is significantly different. While the refracted P wave is partly transferred to the surrounding water and thus, loses energy, the S wave is totally reflected and maintains its initial energy.

For a detailed quantitative study of the amplitudes of the different wave modes, also the third reflection/transmission process at the main face of the prism must be taken into account. Moreover, in addition to the reflection and transmission coefficients with regard to intensity as given by equations (2)-(4), also their counterparts with regard to wave amplitude (like particle velocity or acoustic pressure) must be considered. Unfortunately, this is beyond the scope of the present paper.

From the time-domain signal given in figure 9 the time-of-flight of the mode converted S wave, T_S, can easily be determined. Together with the transit times for the refracted P wave, T_P (from step 2), and that of the reflected P wave, t_P (from step 1), one can deduce a simple formula to determine shear and pressure wave speeds of the prism material by using the specific geometry of the prim (see figure 3). For the transit times $T_{P,S}$ we obtain

$$T_{P,S} = \frac{2R}{c_l} + 2\frac{a/2}{c_{P,S}} = t_P + \frac{a}{c_{P,S}} \quad , \tag{11}$$

and finally for the wave speeds

$$c_{P,S} = \frac{a}{T_{P,S} - t_P} = \frac{a}{T_{P,S} - 2R/c_l} \quad , \tag{12}$$

where a is the side length of the prism. If one is interested in eliminating the dependence on the prism size one could introduce an additional reflector as shown in figure 3, remove the prism and perform another measurement of the transit time t_R of the reflected P wave in water (normal reflection from the reflector). Since the height of the prism is given by $h = a \cdot 2^{-1/2}$ we have

$$t_R = t_P + \frac{2h}{c_l} = t_P + \sqrt{2}\frac{a}{c_l} \tag{13}$$

and together with equation (12) we obtain

$$c_{P,S} = \frac{c_l}{\sqrt{2}} \frac{(t_R - t_P)}{(T_{P,S} - t_P)} = \frac{\sqrt{2}R}{t_P} \frac{(t_R - t_P)}{(T_{P,S} - t_P)} \quad . \tag{14}$$

If we always use a standardized prism size a, distilled water at the same temperature and thus, a constant c_l, as well as a constant R, then the transit times t_P and t_R in equations (13) and (14) can also be seen as characteristic constants of the apparatus. In this case the phase speeds $c_{P,S}$ to be determined are a function of the transit times $T_{P,S}$ only and the formula takes the simple form

$$c_{P,S} = \frac{K}{T_{P,S} - k} \quad , \tag{15}$$

where K and k are characteristic constants of the measurement system.

2. The Apparatus

3.1 System description

The schematic diagram of the ultrasonic testing apparatus is shown in figure 10. It consists of an Ultrasonic Pulser/Receiver (Panametrics 5077PR), various Immersion Transducers (Panametrics, 1-2.5 MHz), a Longitudinal Wave Contact Transducer (Panametrics V106RB), a Digital Oscilloscope (Tektronix TDS 1002), a Laptop Computer with WaveStar software for data-acquisition, and the Transducer Cell.

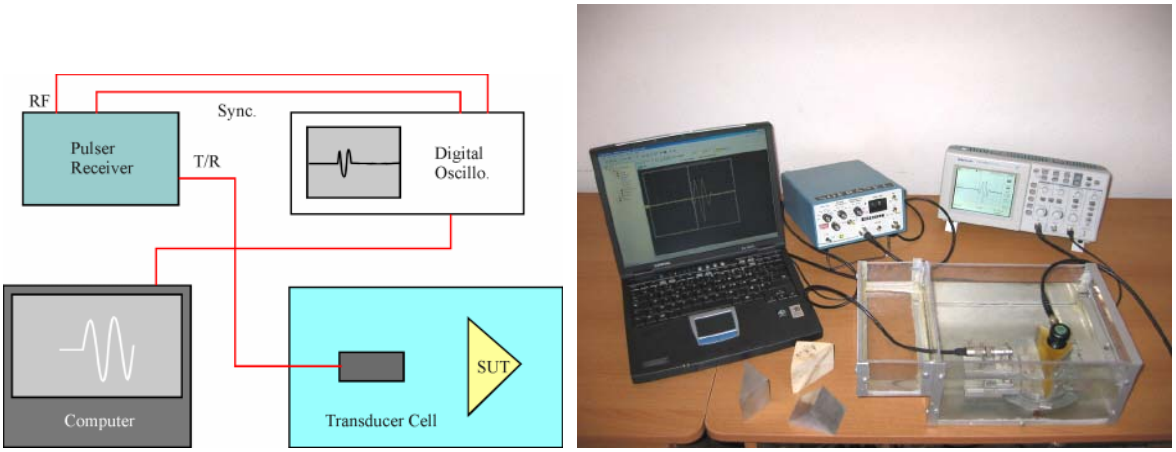

Figure 10: Schematic diagram (left hand side) and photograph (right hand side) of the ultrasonic apparatus.

3.2 System operation

At the start of the experiment, the incident waves from the immersion transducer are made to impinge normally on the largest face (main face) of the prism. The related echo gives the time-of-flight of the wave within the water. Next, the angle of incidence is increased slowly until the disappearance of the first echo and the emergence of a second echo related to refracted P waves. After that, the angle is increased further, a third echo appears, and this time it is related to shear waves within the prism.

The accuracy of measurements depends only on one parameter, namely the time-of-flight of ultrasonic waves. It could be determined with high precision using well-known signal processing techniques, such as the overlap, cross-correlation or cepstrum algorithms. However, since the echoes are quite strong, no complex signal conditioning is required in

most cases. The cursors of the digital oscilloscope were positioned on the main half-cycle of the echo to give a fairly accurate measurement of the transit times.

3.3 Prism samples

Special care must be undertaken while preparing the materials samples. The starting point should be from a perfectly made cube, which has a side length of about 50 mm. It is then divided through its diagonal into two equal prisms. The prism could also be made from a cylindrically shaped specimen. The critical point here is to ensure the right angle between the two side faces.

Unlike cylindrically shaped specimens, the prism-shaped ones could be tested in three different directions, which would give a fairly good idea about the anisotropy of the material. There is also the possibility of crosschecking the velocity of P waves using a contact transducer. Therefore, the drawback related to the difficulty of preparing prism-shaped specimens compared to cylindrically shaped ones is more than compensated by the wealth of information yielded from the former.

3.4 System calibration

A reference prism is made from aluminum. The values of both wave velocities are engraved on the block. It is also used as a reflector for measuring the transit-times t_R and t_P. The Radius R is measured with great accuracy from knowing the velocity of ultrasound in distilled water at a certain temperature and t_P. A second contact transducer that has the same center frequency as the immersion one is used to cross check the P wave velocity before the start of the experiment. The system being temperature compensated is then ready for making the rest of measurement.

3. Experimental results

The waveforms shown in figure 11 are obtained by simply rotating the transducer around the specimen as explained in chapter 2. In this case the specimen is made of Aluminum, and cut from a cube that has a side length of 56 mm. As can be seen from the two lower pictures in figure 11, the echo related to the refracted P wave in the prism is significantly smaller than the echo related to the refracted S wave. In the latter case even multiple echoes can be identified. The observation of a strong S wave echo agrees well with the energy-related considerations done in section 2.3.

From the oscilloscope display the transit times of the different waveforms are determined and the characteristic wave speeds of the prism material can be calculated using equations (13) or (14). From the wave speeds the two Lamé constants of an isotropic medium, λ and μ, as well as Young's modulus E, bulk modulus K, and Poisson's ratio ν_0, can be easily derived by using well-known formulae given in any serious text book. Table 1 shows second-order elastic constants for various materials as obtained by the prism technique.

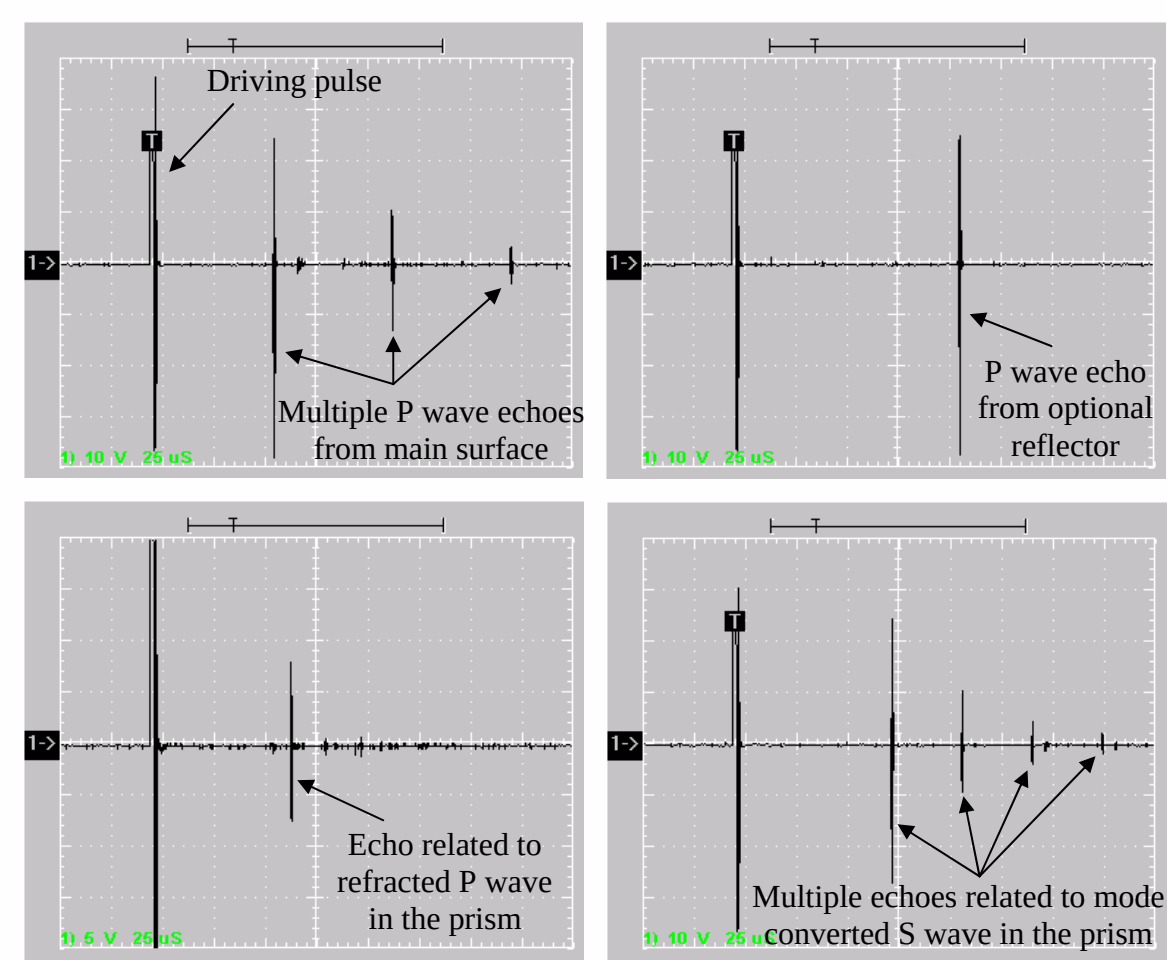

Figure 11: Oscilloscope displays obtained for an Aluminum sample showing multiple echoes from the main face of the specimen (top left), an echo from the optional reflector (top right), an echo related to the refracted P wave in the prism (down left), and multiple echoes related to the mode converted S wave in the prism (down right).

Table 1: Second-order elastic constants as obtained by the prism technique

Material	ρ **(kg/m³)**	c_P **(m/s)**	c_S **(m/s)**	λ **(GPa)**	μ **(GPa)**	E **(GPa)**	K **(GPa)**	ν_0 **(GPa)**
Aluminum 2017A	2764	6380	3048	61.2	25.7	69.4	78.3	0.352
Brass	8782	4271	2127	80.7	39.7	106.1	107.2	0.335
Mortar (w/c=0.55) (s/c =1)	2006	3387	2072	5.8	8.6	20.7	11.5	0.201
Mortar (w/c=0.35) (s/c=1)	2133	3950	2355	9.6	11.8	29.0	17.5	0.224

4. Discussions and outlook

This experiment shows that it is possible to measure both P and S wave velocities of the prism material with relative ease. Material samples are easy to prepare and only one variable is needed for computing the elastic constants, namely the transit-time of the ultrasonic pulses. The latter are measured with the digital oscilloscope using the vertical cursors. The accuracy is directly related to the sampling rate of 1 Gsamples/second, which gives a definition of one nanosecond. This is more than enough for the measurement of velocities, which are needed for the determination of second-order elastic constants. However, this will be crucial when the same apparatus is used for detecting small changes in wave speed due to nonlinearity induced by external stress, which could be generated by applying uniaxial and hydrostatic pressures on the specimen. This means that the present method could be easily extended to the determination of third-order elastic constants.

The main advantages of this method over other more known ultrasonic techniques and especially the rotating plate technique (which shares some of the features) are as follows:

- There is just one transducer used for measuring the wave speed of both compressional and shear waves.
- Easy and uniform coupling between the transducer and the sample, which characterizes immersion-testing methods
- The measured velocities are independent of the exact incidence angle, which represents a huge advantage over goniometer methods.
- Measurements are temperature compensated, which means that the wave speed remains constant for small variations around the ambient temperature. However, the liquid interface could be used to transfer heat to the sample for taking measurements at high temperatures.
- The same configuration could be easily adapted to test samples under high stresses (uniaxial compression, hydrostatic pressure, etc.).
- Due to the strong echoes no complex signal processing is required in general.

Finally we would like to mention that the proposed prism technique could also be used to measure attenuation characteristics of the prism material in principle. This damping can be caused by viscoelastic dissipation, scattering by aggregates and pores as well as by nonlinear effects. For this kind of measurement a detailed quantitative analysis of expected amplitudes including compensation of system-related attenuation (geometrical spreading and damping in water) is needed. This topic is the subject of ongoing research and will be published elsewhere.

References

[1] J Krautkrämer and H Krautkrämer, ‘Ultrasonic Testing of Materials’, Berlin (Springer-Verlag), pp 529-539, 1990.

[2] J Blitz and G Simpson, ‘Ultrasonic Methods of Non-Destructive Testing’, London, (Chapman&Hall), pp 85-108, 1996.

[3] R Bar, Helv Phy Acta, Vol 13, p 61, 1940.

[4] WC Schneider and CJ Burton, ‘Determination of the Elastic Constants by Ultrasonic Methods’, J Appl Phys, Vol 20, pp 48-58, 1949.

[5] M B Reynolds, ‘The Determination of the Elastic Constants by the Ultrasonic Pulse Technique’, Trans Am Soc Metals, Vol 45, pp 839-861, 1953.

[6] B R Rao and P V Rao, Nature , Vol 174, p 835, 1954.

[7] M A Breezeale and EA Hiedemann, J Acoust Soc Am, Vol 27, p 1220, 1955.

[8] W Mayer, ‘Energy Partition of Ultrasonic Waves at Solid-Liquid Boundaries’, Ultrasonics, Vol 3,

pp 62-68, 1965.
[9] K Ergin, 'Energy Ratio of the Seismic Waves Reflected and Refracted from Rock-Water Boundary', Bull Seism Soc Am, Vol 42, pp 349-372, 1952.
[10] L Brekhovskikh, 'Waves in Layered Media', Academic Press, NewYork, 1960.
[11] F Rollins, 'Critical Ultrasonic Reflectivity – a Neglected Tool for Material Evaluation', Material Evaluation, Vol 24, pp 683-689, 1966.
[12] L S Fountain, 'Experimental Evaluation of the Total Reflection Method of Determining Ultrasonic Velocity', J Acoust Soc Am, Vol 42, pp 242-247, 1966.
[13] F R Rollins, 'Ultrasonic Examination of Liquid-Solid Boundaries Using a Right-Angle Reflector Technique', J Acoust Soc Am, Vol 44, pp 431-434, 1968.
[14] A R Gregory et al, 'Dual-Mode Ultrasonic Apparatus for Measuring Compressional and Shear Wave Velocities of Rock Samples', IEEE Trans Sonics and Ultrasonics, Vol 17, pp 77-85, 1970.
[15] R A Kline, 'Measurement of Attenuation and Dispersion Using an Ultrasonic Spectroscopy Technique', J Acoust Soc Am, Vol 76, pp 499-505, 1984.
[16] J Wu, 'Determination of Velocity and Attenuation of Shear Waves Using Ultrasonic Spectroscopy', J Acoust Soc Am, Vol 99, pp 2871-2875, 1996.
[17] R J Freemantle and R E Challis, 'Combined Compression and Shear Wave Ultrasonic Measurements on Curing Adhesive', Meas Sci Technol, Vol 9, pp 1-12, 1998.
[18] D E Bray, 'Current Directions of Ultrasonic Stress Measurement Techniques', 15th WCNDT, Rome, 2000.
[19] I Anto et al, 'An ultrasonic Method for Determination of Elastic Moduli, Density, Attenuation and Thickness of a Polymer Coating on a Stiff Plate', Ultrasonics, Vol 39, pp 211-221, 2001.
[20] I Imamura, 'Measuring Method for the Mechanical Anisotropy of Solid by Water Immersion Ultrasonic Sing-Around Method', 3rd World Congress Ultrasonics, Paris, 2003.
[21] A Bouhadjera, 'A Universal Ultrasonic Apparatus for Measuring Elastic Constants of Materials', PhD Thesis, Nottingham Univ, England, 1988.
[22] A Bouhadjera, 'A Mode Conversion Method for Evaluating Elastic Properties of Materials', Insight, Vol 38, pp 732-736, 1996.
[23] A Bouhadjera, 'An Improved Design of an Ultrasonic Apparatus for Characterizing Material Samples', Insight, Vol 46 N°9, pp 554-558, 2004.
[24] A Bouhadjera and C. Bouzrira, 'High-Frequency Ultrasonic Testing of Young Cement-based Materials Using the Prism Technique', NDT&E International, Vol 38, pp 135-142, 2005.
[25] V A Sutilov, *Physik des Ultraschalls*, Akademie-Verlag Berlin, 1984 (in German).
[26] F Schubert, 'Numerical Time-Domain Modeling of linear and Nonlinear Ultrasonic Wave Propagation using Finite Integration Techniques – Theory and Applications', Ultrasonics, Vol 42, pp 221-229, 2004.